Exploiting generative design for multi-material inkjet 3D printed cell instructive, bacterial biofilm resistant composites

Yinfeng He[1] †, Belen Begines[2] †, Gustavo F. Trindade[1,3], Meisam Abdi[4], Jean-Frédéric Dubern[5], Elisabetta Prina[3], Andrew L. Hook[3], Gabriel Choong[1], Javier Ledesma[1], Christopher J. Tuck[1], Felicity R. A. J. Rose[6], Richard Hague[1], Clive J. Roberts[3], Davide De Focatiis[1], Ian A. Ashcroft[1], Paul Williams[5], Derek J. Irvine[1], Morgan R. Alexander[3], Ricky D. Wildman[1*]*

[1]Faculty of Engineering, University of Nottingham, University Park, NG7 2RD, Nottingham.

[2]Department of Organic and Medicinal Chemistry, School of Pharmacy, University of Seville, Seville, 41012, Spain

[3]Advanced Materials and Healthcare Technologies, School of Pharmacy, University of Nottingham, NG7 2RD, UK

[4]School of Engineering and Sustainable Development, De Montfort University, LE1 9BH, Leicester

[5]National Biofilms Innovation Centre, University of Nottingham Biodiscovery Institute, School of Life Sciences, University of Nottingham, NG7 2RD, United Kingdom

[6]University of Nottingham Biodiscovery Institute, School of Pharmacy, University of Nottingham, University Park, Nottingham, NG7 2RD, UK

† These authors contributed equally to this work

Keywords: Multimaterial, 3D printing, Generative design, Cell instructive, Bacterial biofilm resistant

*correspondence to: Ricky.Wildman@nottingham.ac.uk and Morgan.alexander@nottingham.ac.uk

Abstract

As our understanding of disease grows, it is becoming established that treatment needs to be personalized and targeted to the needs of the individual. In this paper we show that multi-material inkjet-based 3D printing, when backed with generative design algorithms, can bring a step change in the personalization of medical devices. We take cell-instructive materials known for their resistance to bacterial biofilm formation and reformulate for multi-material inkjet-based 3D printing. Specimens with customizable mechanical moduli are obtained without loss of their cell-instructive properties. The manufacturing is coupled to a design algorithm that takes a user-specified deformation and computes the distribution of the materials needed to meet the target under given load constraints. Optimisation led to a voxel map file defining where different materials should be placed. Manufactured products were assessed against the mechanical and cell-instructive specifications and ultimately showed how multifunctional personalization emerges from generative design driven 3D printing.

Introduction

Recently, libraries of materials showing cell-instructive properties have been identified for a range of functionalities. These have included those that resist bacterial biofilm formation, promote mesenchymal stem cell attachment and the prevention of fungal proliferation[1-4]. The generation of these libraries aims to provide a suite of selectable materials suitable for components or devices that seek to direct cellular behaviour. A limitation of this approach is that it is usually restricted to the material properties 'as received', and further formulation is needed to achieve the desired processability[5,6], thus giving rise to potentially detrimental effects on the cell-instructive and mechanical behaviours. This can be avoided if we exploit the design freedoms of 3D printing: in addition to the well understood concept of customized geometry, Multi-Material Inkjet 3D Printing (MM-IJ3DP) allows us to spatially vary the material composition and thus include differentiated functionalities[7-9]. MM-IJ3DP can be used to directly produce 3D objects with high resolution and production speeds and, importantly, with a high degree of control over material composition. In principle, material composition can be varied on a voxel or droplet basis. which opens the possibility of a next generation of 3DP that allows the user to produce devices with spatially distributed, customizable material functionalities in a cost-effective manner [10-14].

This paper sets out to develop a platform by which MM-IJ3DP can be used to create bespoke devices with tuneable, spatially varying mechanical performance, whilst incorporating and retaining cell-instructive functions - in this case resistance to bacterial biofilm formation. Recent work has demonstrated the formulation of established cell-instructive materials[1,2] into printable inks for IJ3DP, where the functional behaviour was retained, thus exploiting the geometrical freedoms of IJ3DP to create bio-relevant products[15]. This work goes significantly beyond this concept by using a computational design approach to direct the manufacture of multi-material devices – specifying where materials with different moduli need to be deposited in order to achieve a customised deformation for a given loading case. Further, we show that the use of MM-IJ3DP

results in a complex interface / interphase at the junction between drops showing an interpenetrating layer which promotes intimate contact between two adjacent material drops.

To demonstrate the benefits for designing and manufacturing using MM-IJ3DP, we chose an exemplar which was inspired by the opportunity to address antimicrobial resistance through the implementation of (non-killing) bacterial biofilm-resistant materials. Prevention of bacterial biofilm formation at the surfaces of medical devices is of particular relevance for diverse biomedical applications. Biofilms are communities of bacteria sequestered within a self-produced extracellular matrix that achieve up to 1000 times greater tolerance to antibiotics and host immune system defences[16] and are a major unsolved biomedical problem that accounts for 25.6% of all healthcare-associated infections within the USA[17]. The incorporation of antibiotics is widely used to reduce device infections, but is often accompanied by localized cytotoxicity[18], active component depletion[19,20] and selection for resistance imposed by the bactericidal nature of most antimicrobial agents[21]. A library of materials that exhibits resistance to bacterial biofilm formation without killing bacteria so facilitating immune clearance has recently been developed[2]. These materials were selected for use in this study.

We developed two functional ink formulations that inhibit biofilm formation after polymerization whilst having highly differentiated elastic moduli (Fig. 1a). Backed by a pseudorandom co-deposition polymerization printing strategy, complex 3D structures with the required spatially dependent compliance were manufactured (Fig. 1b and c). We then invoked computational modelling as a design tool. On this basis, devices with a bespoke mechanical performance could be designed and then manufactured through MM-IJ3DP (Fig. 1e). A selection of characterization methods was included to investigate the physical and biological performance of our designed specimens, resulting in confirmation that our multi-material constructs performed as expected mechanically, and retained their cell-instructive function (Fig. 1d)

Results

Development of ink formulations and printing strategy for MM-IJ3DP

Novel reactive ink formulations were developed and optimized for the MM-IJ3DP process to produce structures with distinct mechanical performance (rigid and flexible) while possessing resistance to bacterial attachment. A selection of monomers from the candidate library[2] were investigated whilst considering reactivity, biofilm inhibition, processability and mechanical properties. Informed by this, two MM-IJ3DP ink formulations (ink A and ink B) were successfully formulated by a process which selected combinations of materials to enable cell instructive performance, whilst allowing for printability and a range of mechanical behaviours. Ink A formed a rigid polymer after printing and consisted of 50 v/v% ethylene glycol dicyclopentenyl ether acrylate (EGDPEA) and 50 v/v% tricyclo decanedinmethanol diacrylate (TCDMDA) as structural monomers. Both EGDPEA and TCDMDA have been confirmed to inhibit *P. aeruginosa* and *S. aureus* biofilm formation when polymerized [1,2]. Ink B contained 60 v/v% 2-ethylhexyl acrylate (EHA) and 40 v/v% hydroxybutyl acrylate (HBA) and was formulated to produce a flexible material. The glass transition point (T_g) of the polymers was taken into consideration when selecting the components for ink B with a guide that those with a T_g lower than room temperature tend to be flexible at that temperature[22], and those higher are more rigid (Supplementary Table S1). Poly-EHA is a candidate (T_g ~ -70°C) for inhibition of biofilm formation of both bacterial strains[2], but EHA is not suitable for inkjet printing due to its viscosity, reactivity and volatility. Consequently, we added HBA to aid the printing, since HBA has a similar T_g and preliminary inkjet printing trials had shown it to be printable. 2,2 Dimethoxy-2-phenylacetophenone was chosen as the photoinitiator as it was soluble in both ink formulations. The rheology of the inks was determined, and the printing parameters tailored to ensure reliable printing (Supplementary Fig. S1/S2, Table S2).

Printing was carried out using a PiXDRO LP50 printer (Meyer Burger) equipped with a Spectra 128SE dual head assembly and a UV lamp (365nm, 900mW/cm^2). Each layer was divided into two

sub-patterns (A and B) and assigned to different printheads for ink A and B (Supplementary Fig. S3). A pseudorandom pixel deposition strategy using Mathematica (v10.4) was used to create a different pattern for each layer, whilst keeping the fraction of A and B constant. Ink A was deposited first, with Ink B second, 'filling in' the gaps left by Ink A. This process avoided pattern replication and minimized any unintended inhomogeneity of material properties. The pseudorandom co-printing strategy was tested using two coloured commercial inks and created a simple gradation in colour. Thus, printing a whole layer consisted of four steps: 1) printing of ink A; 2) application of UV light for pinning (1 s); 3) printing of ink B; 4) application of UV light for curing (25 s). From this point onwards, all the polymer samples were named as 'A' plus number (1-100) representing the ratio of ink A in the composite, e.g. A25 (25% pixels filled with ink A and 75% filled with ink B).

Modulus range of MM-IJ3DP printed cell-instructive composite

Having established the printing strategy and formulation of the composite, it was necessary to determine and codify the relationship between composition and mechanical properties – this would allow a 'dial up' of mechanical composition through selection of the balance of ink A and B using our calibration curve. Polymer composite strips (5 x 20 x 1 mm^3) with 10 different ratios of A to B were produced. The samples were measured using dynamic mechanical analysis (DMA) at 25°C. Fig. 2a shows that it was possible to manipulate the modulus of the polymer composition by tuning the ratio of ink A and ink B, resulting in an available storage modulus ranging from 1.3 MPa (A12.5) up to 2300 MPa (A100). It was found that the relationship of storage modulus to the proportion of ink A was non-linear.

A subsequent study using thermo gravimetric analysis (TGA) was performed to understand further the nature of the printed composite (Fig. 2b, Supplementary Table S3). Pure Ink A (A100) and Ink B (A0) were tested as control samples, which showed maximum decomposition rate was reached

at temperatures of 468ºC and 414°C respectively. According to the TGA results from printed composite specimens with 25 v/v% (A25), 50 v/v% (A50) and 75 v/v% (A75) of ink A, the decomposition temperature increased as the proportion of ink A increased. Further derivative analysis of the curve highlighted this trend (Fig. 2c). Proportion normalized A100 and A0 curves were subtracted from the correlated composite curves, which revealed a signal hitherto not seen (Supplementary Fig. S5)

Interaction of the co-printed ink phases

On the scale of single droplets, our fabrication methods do not produce homogenous distributions of A and B – drops of material are contiguous. It is therefore necessary to understand the nature of the interaction at the junction of two dissimilar drops. For this, we exploited time-of-flight secondary ion mass spectrometry (ToF-SIMS) 3D analysis to investigate the homogeneity of the co-printed polymer composite structure (Fig. 3a). Spectra of the individual inks were acquired to identify exclusive signals for each of the formulations via the unsupervised machine learning method 'non-negative matrix factorisation' (NMF) of a joint dataset containing spectra of the individual inks as well as spectra of the mixed sample at various depth profiling levels[23] (more details in Supplementary Fig. S4). From NMF endmembers, the secondary ion $C_7H_7^+$ (91.07 u) was chosen to represent the cyclic structure of monomer EGDPEA of ink A and $C_3H_7^+$ (43.06 u) to represent propyl end groups of monomer EHA of ink B. Clear separation between ink A (purple) and B (green) was observed in the 3D depth profiling (Fig. 3a), with ink B filling up the gaps designed between ink A and covering most of the top surface – a consequence of the sequential printing strategy of printing and pinning drops of ink A, then depositing and curing drops of ink B. Upon further investigation of the spatial intensity distribution of the NMF endmembers representing the two inks, using a 80 % / 20% definition of the edge spread function[24,25] we could determine that the interface (Fig. 3b and c) within the observation area has an average width of 16.7 ± 4.3 μm

(Fig. 3d), which indicates that there was interpenetration during the printing and curing process. The combination of TGA derivative data and ToF-SIMS analysis of the interface suggests that the interface is composed of both A and B, predominantly in the form of physical interfacial mixing of molecules of A or B, with the TGA analysis pointing towards the possibility of some chemical copolymerisation of A and B into a new material. However, the ToF-SIMS analysis was not able to resolve the difference in these states and further investigation is required to conclusively determine the chemical composition of the material at the interface.

Bacterial biofilm inhibition assessment of printed composites

A bar specimen (7 x 2 x 2 mm^3) containing three sections of different compositions (A25, A50 and A75) were printed and incubated with bacterial strains to assess their biofilm inhibition performance (Fig. 4a). The human opportunistic pathogens *P. aeruginosa* (gram-negative) and *S. aureus* (gram-positive) were selected as they are frequently linked with medical device-associated infections such as those on implanted prostheses and often result in poor clinical outcomes [26,27]. Both bacterial strains, tagged with fluorescent proteins were incubated with the printed specimens containing three sections of different compositions (A25, A50 and A75) for 72 h to allow biofilms to establish. The coverage and biomass of *P. aeruginosa* and *S. aureus* biofilms were quantitatively assessed by confocal fluorescence microscopy. The results revealed that all the printed compositions inhibited biofilm formation for both pathogens in comparison with silicone rubber (Appleton Woods medical grade tubing), a commonly used polymeric biocompatible material used for medical devices. Compared with silicone rubber, *P. aeruginosa* showed 76.4 ± 3.0%, 63.4 ± 6.0% and 21.9 ± 7.4% biofilm biomass reduction on A75, A50 and A25 respectively, while for *S. aureus*, the reductions were 75.2 ± 8.7%, 61.7 ± 10.3% and 28.5 ± 10.7%. As the proportion of ink A increased, the composite material showed greater resistance to biofilm formation. Previous assessments[2] indicated that the components of ink A are more effective at resisting colonisation

than ink B, and thus these observations align with those findings. Ink B, although not as effective as ink A against biofilm formation, still performs better than the current standard (silicone) and can thus still be used to reduce modulus while increasing flexibility, whilst not substantially degrading the cell-instructive function of the composite. However, when implementing finite element (FE) assisted generative design as a tool, we attempted to constrain the material composition to include ink A as the major component in order to maximise biofilm inhibition.

Mammalian cell response experiments

The potential mammalian cell cytotoxicity of the printed material is a primary consideration for whether a printed device is biocompatible for clinical applications. The evaluation of the *in vitro* cytotoxicity and cell attachment test was performed by growing immortalized NIH 3T3 mouse embryonic fibroblast cells in contact with the material indirectly or directly (Fig. 4c and d) following ISO standard 10993 [28]. There was no cytotoxic leaching for A50 and A100, while A0 presented 20% cytotoxicity until day 8 (Supplementary Fig. S6 and S7). The chosen cells adhered and proliferated on all the samples. Cells presented the lowest values of proliferation on A0 within the testing period and a less uniform distribution. The Live/Dead results confirmed the majority of the cells were viable, presenting an elongated morphology and covering the entire specimen.

Designing multi-material response through MM-IJ3DP

The establishment of the relationship between compositions and moduli, combined with the ability to selectively deposit material spatially, enables the user to control the response of an object in a 'non-trivial' way: by varying the distribution of material voxels, and therefore the modulus, on demand across the object. We demonstrate this capability in two steps: first by showing that it is possible to adjust the location of a flexural region in order to provide a 'hinge' in any desired location[29-31]; secondly, by using a material optimisation approach to show that it is possible to seek

a user defined beam deformation profile under a fixed loading condition by spatially varying the composition distribution of the beam only.

In the first instance, we chose a cantilever beam and sought to demonstrate a hinge-like functionality that could only be achieved when using a homogenous distribution of material by creating a narrow, and consequently weak constriction in the beam. A simple cantilever (25 mm(L) x 5 mm(W) x 0.4 mm(H)) was printed that consisted of 80 v/v% A75 and a short section of 20 v/v% A12.5 (Fig. 5a and b). The 'hinge' region (4 mm(L) x 5 mm(W) x 0.4 mm(H)) was shifted by moving the location of the flexible A12.5 segment from 15 mm from the leftmost, i.e., free end in Fig 5a to 10 mm from the free end in Fig 5b. The data shows that when applying a fixed vertical displacement of 5 mm to the free end, we were able to create a deformation hinged at a specific location by varying the flexible segment location. Such a technique would be applicable to a finger joint prosthetic for example. Current products on the market are 'hinged' using a narrow section that allows for a bending motion. However, we also show that this may be achieved through a novel materials composition optimisation approach, avoiding the requirement for a thin section and maintaining a bulk section for strength. Further, this device was manufactured using the materials selected for their resistance to bacterial attachment (Fig. 5c), an important sought-after feature that can reduce infection rates during and post-surgery. The use of this material illustrates how other, non-mechanical, functionalities can be incorporated into our design and materials selection methodology.

To show the further opportunities for design via material optimisation, we developed a computational model of multi-material structures and assessed by three-point bending. This was created in Matlab (R2017a) using a FE model constructed from quadrilateral elements. Each finite element was assumed to be formed from a homogenous material with a composition varying from A12.5 to A100. Sixteen different possible compositions within this range were chosen and their associated moduli were derived from fitting a curve to the experimental measurement of moduli in

Fig. 2a. The customized multi-material sample model used in this study, as a demonstration, was a simply supported beam (with average composition of A66) which was designed to exhibit a deformation close to 0.250 mm at the centre when it is subjected to a point load of 2 N. The system was implemented under the constraint of a fixed average material composition (A66), which in this case was inspired by the need to weight the amount of biofilm resistant material in the composite towards ink A (Fig. 4a).

An elastic material model was implemented with an objective function defined to minimize the root mean square difference between the displacement magnitude of the FE nodes (U_{FEM}) and the displacement magnitude of corresponding points on an imposed grid on the desired deformation profile (U_{des}):

$$\text{Minimize } \Delta = \sqrt{\frac{1}{n}\sum_{i=1}^{n}(U(i)_{FEM} - U(i)_{des})^2}$$

where *n* denotes the number of FE nodes. The objective function defined in the equation above aims to minimise the difference between FE nodal displacements and the displacement of the control points on the desired deformation profile. This was achieved by spatially varying the material composition of finite elements in FE model of the beam iteratively through a Genetic Algorithm (GA). The convergence happened when generation of the new designs was not significantly different from the previous generation. Upon completion of the iterative steps and convergence of the optimization, our model provided a distribution of material composition corresponding to the elements of the FE model. This predicted distribution of material was tested by replicating this distribution in samples produced using our MM-IJ3DP approach (5 x 2 x 0.7 mm^3). These printed samples were tested experimentally using a flexural test fixture [32] identical to that used in the model. When the prescribed deflection (0.250 mm) was reached at the centre of the bespoke specimen beam, the observed load was 2.12 ± 0.22 N, in agreement with the designed load (2 N). As a comparison, a homogeneous cantilever with the same average composition would deflect by 0.145 mm under the same loading conditions (Fig. 6a). The ink A and B distribution in

both the homogeneous cantilever and the designed version is presented in Fig. 6b, while Fig. 6c gives a comparison of their deformation profiles.

Discussion

This work has demonstrated the manufacture of multi-material 3D printed devices that are personalisable through judicious choice and distribution of inks to create materials that are both resistant to bacterial biofilm formation and achieve a specific deformation profile. Our studies showed that it was possible to combine two materials to create a composite that, upon choice of suitable composition ratios, possessed moduli ranging from that of the low modulus material (1.3 MPa) to that of the high modulus material (2300 MPa). Our design tools show that using a multi-material approach to achieve spatial organisation of the varied components, we can achieve non-linear deformations that are not readily accessible when using single materials. Inspection of the composite at the sub-voxel / droplet level showed that an interphase region formed at the expected interface. In this region we saw evidence of physical intermixing at the molecular level. Further study is needed to confirm the existence or not of covalent bonding between the two inks in this region. This creation of a composite of material by design allows the development of sophisticated products where function is distributed throughout the component in a single step of manufacture. Our design tools demonstrated the creation of simple hinges in precise locations as well as deformation profiles that would not be accessible from the homogenous material, under the same loading case. Our combined use of advanced formulations and design led MM-IJ3DP substantially advances our ability to deliver personalised medical devices that have biological and deformation profiles tailorable to individual patient requirements.

Materials and Methods

Ink preparation and assessment

For ink preparation, 20mL of ink was prepared each time. A corresponding amount of photoinitiator was added in the right combination of monomers and the mixed at room temperature at 800rpm using PTFE coated magnets (10mm) till it is fully dissolved. The formulation was then degassed with a N_2 flow for 15 min.

Monomers and initiator were purchased from Aldrich Chemical Co. and used as received. Viscosities were estimated using a Malvern Kinexus Pro Rheometer equipped with a parallel plate at 300 µm separation, under shear rates from 10 s^{-1} and 1000 s^{-1}. Each measurement started at 25ºC with 5ºC increments up to 60ºC, the precise increments depending on the sample. A protocol of waiting 300 s after reaching the test temperature was set to ensure the ink was in a steady state condition. At each temperature point and shear rate, the viscosity was recorded at 5 s intervals within a 180 s test time.

Parameters and machine set up for MM-IJ3DP

Samples inkjet printing was performed using a piezoelectric inkjet printer (PiXDRO LP50, Meyer Burger) fitted with a dual head assembly and two printing heads with 128 nozzles (Spectra® SE-128 AA, Fujifilm Dimatix, Santa Clara, USA), set at 55°C for ink 1 and 25°C for ink 2. The diameter of the nozzles was 35 µm and the nozzle spacing was 508 µm. Heads assembly was equipped with a UV LED radiation source, with a maximum peak at 395 nm. The emission window was 25 mm x 10 mm with an emitted energy of 7 W/cm^2. Printing was done on polyethylene terephthalate (PET) substrate with a set temperature of 25°C. The whole system was installed inside a glovebox with O_2 < 300 ppm and a temperature lower than 30°C. Printing parameter optimisation were optimised using Advanced Drop Analisys (ADA) Flexibleware provided by Meyer Burger. Bitmaps were created using Wolfram Mathematica 10.4.

Material Characterisation

To assess layer thickness for a representative set of formulations, surface profiles were obtained using a Bruker Contour GT-K Interferometer, equipped with a 5X lens amplified 2X. Vision64TM Flexibleware was used to analyse images, obtaining the values for average height.

Dynamic Mechanical Analysis (DMA) tests were carried out at room temperature using a Perkin Elmer DMA 8000 in tension mode. Specimens were printed following a rectangular pattern (20 mm in length and 5 mm in width) with 100 layers. The test length was set to 10 mm and the width and thickness of each sample was measured prior to calculating its modulus. The test period was set to 10 min at a frequency of 1 Hz and 0.1% strain. The 3-point bending tests were carried out with a custom-built flexural test fixture [32] at ambient conditions. The thickness of the printed sample was measured by optical microscope picture of sample fractured within liquid nitrogen. Tests were performed at a strain rate of 1.8×10^{-3} s^{-1} until failure. An average of six specimens were tested for each composite formulation. Thermogravimetric analysis (TGA) was performed using TGA4000 (PerkinElmer®) under air environment with a heating program from 50ºC - 600ºC, at the rate of 20ºC/min.

Time-of-flight secondary ion mass Spectrometry (ToF-SIMS) was carried out using a 3D OrbiSIMS (Hybrid SIMS) [33] instrument from IONTOF GmbH (Muenster, Germany). Each secondary positively charged ion spectra was acquired in delayed extraction mode using a 30 keV Bi_3^+ primary ion beam delivering 0.3 pA. For the surface spectra, the primary ion beam was raster scanned over different areas areas with the total dose kept under the static limit of 10^{13} ions/cm^2. The depth profiling data was acquired using a dual-beam fashion by raster scanning the primary ion beam over regions of 300 x 300 μm^2 at the centre of a 500 x 500 μm^2 crater formed using a 20 keV Ar_{2000}^+ ion beam delivering 5 nA. The analysis was performed in the “non-interlaced” mode with a low-energy (20 eV) electron flood gun employed to neutralise charge build up. One sputter frame was

performed per cycle and the pause time per level was set 0.5 s. The ToF analyser was set with 200 µs cycle time, resulting in a mass range between 0 and 3493 mass units. All 3D intensity maps were produced using the simsMVA software [34]. Voxel intensities were normalised by total ion counts to correct for topographic features and the final 3D representations were created by combining isosurfaces ranging from 40% to 90% of the maximum intensity for each ion. Multivariate analysis was carried out using masses as the variables and each spectrum in the depth profile sequence as the observations. For dataset, Surface Lab 7.1 (IONTOF GmbH) was used to perform an automated peak search on the total spectra restricted only to peaks with intensity higher than 100 counts and masses between 30 u and 300 u. Dead-time corrected peak areas were then exported for each pixel of all mapping datasets. Non-negative matrix factorisation (NMF) was performed using the simsMVA software[34] using the stitch function to perform matrix augmentation and create a single matrix containing all (stitched) depth level maps and the reference images, enabling the entire dataset to be processed as a single matrix with pixels in rows and peak intensities in columns. The insertion of rows containing measurements reference materials has proven to be an effective way to identify mixed materials in an unsupervised fashion. More details of the methodology can be found in previous work [23]. Initial conditions were determined by principal component analysis (PCA) and Prior to NMF, data was Poisson scaled to account for heteroscedasticity [35]. After 500 iterations, the analysis yielded the spatial intensity distribution of 2 endmembers with groups of secondary ion peaks that shared the same intensity spatial distribution, relating to inks A and B (Supplementary Fig. S4). The endmember intensity maps were normalised by total intensity and smoothed using a gaussian kernel with standard deviation of 0.5 pixel.

Glass transition point of the pure samples were measured by differential scanning calorimetry (Perkin Elmer DSC 8000) with standard aluminium pan (Perkin Elmer). The temperature range was -85°C to 200°C with 5°C/minutes heating speed and nitrogen protection (20 mL/minute)

Bacterial Biofilm formation

P. aeruginosa PAO1 (Washington sub-line) labelled with mCherry (pMMR) and *S. aureus* SH1000 labelled with GFP (pBK-miniTn7-egfp) were routinely grown on either LB (Luria-Bertani, Oxoid, UK) agar plates at 37 °C or in broth at 37 °C with 200 rpm. After overnight incubation bacteria were pelleted by centrifugation at 9500 rpm for 5 min and resuspended in RPMI 1640. Samples for biofilm attachment assessment were UV sterilised for 10 min prior to use. Bacteria were diluted in RPMI-1640 to an OD600 = 0.01 and incubated with samples for 72 h at 37 °C and shaken at 60 rpm. Samples were washed 3 times with 10 ml of phosphate buffer saline for 5 min on a rocking platform at 60 rpm before blotting and air drying. Samples were imaged by confocal microscopy using a Carl Zeiss LSM 700 laser scanning confocal microscope fitted with 488 nm and 555 nm excitation lasers and a 10x/NA 0.3 objective. Images were acquired using ZEN2009 imaging software (Carl Zeiss). Bacterial biofilm surface coverage was quantified using Image J 1.44 software (National Institutes of Health, USA) and Comstat B [36]

Cell response experiments

Cell culture medium was prepared by adding by adding 10% (v/v) of Foetal Bovine Serum (Sigma-Aldrich, UK), 2 mM L-glutamine (Sigma-Aldrich, UK) and 100 U/mL penicillin, 0.1 mg/mL streptomycin and 0.25 µg/mL amphotericin B (Sigma-Aldrich, UK) to Dulbecco's Modified Eagle Medium (DMEM, Sigma-Aldrich, UK). The samples (0.7 x 0.7 x 1.5 cm) were sterilized by UV radiation for 10 min (UVP, Upland CA, USA, Cambridge, Black-Ray XX-15L UV bench Lamp). After sterilisation, specimens were washed three times for 5 minutes each with Phosphate buffered saline (PBS, Sigma-Aldrich).

Extract cytotoxicity test [37]: The samples were placed in 48 well plate and 400 µL of cell culture media was added to each sample. The extracted media were collected after 1 day, 3 days, 5 days and 8 days. At each time point 200 µL of fresh media were collected and substituted with 200 µL

of fresh media. Immortalized NIH 3T3 mouse embryonic fibroblast cells (3T3s) (passage 60) were seeded in 96 well plate at a density of 5000 cells/well (100 µl). At an 80% confluency, the cell culture media were substituted to extract media of all time point and incubated for 24 h at 5% CO2, 37°C, according to the ISO standard 10993-5:200(E). Cells cultured in cell culture media were considered as a control. Lactate dehydrogenase assay (LDH Assay kit, Thermo Scientific) and PrestoBlue® assay (Invitrogen) were used to test the cytotoxicity of the extract media and the cell viability, respectively. Both tests were performed according to the manufacturing protocols. Briefly, the LDH activity was measured by reading the absorbance at 490 nm (subtracted to the 680 nm) by Spectrofluorometer (Tecan Infinite M200 microplate reader). The results were compared to the maximum LDH activity, where 10 µl of Lysin Buffer (10X) was added to the cells for 30 min before performing the test and the Spontaneous LDH activity, where cells were growth in normal media. PrestoBlue solution was diluted 1:10 in cell culture media and added to the microplate wells. After 45 min the fluorescence intensity of the solution, which is proportional to the cell metabolic activities, was measured at an excitation/emission wavelength of 560/590 nm, respectively, and each value was subtracted to the blank sample (media without cells).

Direct cytotoxicity. The samples were placed in a 24 well plate and 1 mL of cell culture media was added for 24 h. 3T3 cells were seeded over materials surfaces at a concentration of 80000 cells/well (0.5 mL). After 24 h, samples were transferred to a new plate and 1:10 PrestoBlue® solution added. Fluorescence intensity was measured at 560 and 590 nm, corresponding to excitation and emission wavelengths, respectively, and each value was subtracted to the blank. The test was performed after 1, 3, 5 and 7 days. For each time point, LIVE/DEAD® Kit (Invitrogen, UK) was performed. Calcein AM (2.5 µM) and Ethidium homodimer-1 (5 µM) were added and samples incubated for 30 min at 37°C at 5% CO_2. Images in green and red channels were taken by fluorescence microscope (Lumen Dynamics Leica DMIRB, USA equipped with X-Cite® Series 120 Fluorescence Illuminator, Excelitas Technologies).

Finite Element Assist Optimization

During the optimization process, an assumption was applied that the storage modulus measured in a DMA test at 1Hz and 0.1% strain is equal to the bending modulus in the elastic region. This model was applied to the cantilever test and the predicted deformation profile fitted the experimental data. A Genetic Algorithm (GA) was employed to find the optimized spatially dependent material composition within the device for an intended objective (that would not be achievable with a homogenous material under the same loading conditions). In this work, the FE model of the beam was constructed from 20x2 quadrilateral elements (21x3 FE nodes, i.e. n=63). Therefore, the desired deformation was described by defining displacement values of 21x3 control points (associated with the 21x3 FE nodes) on the desired deformation profile (U_{des}). Within GA, an initial population of 200 designs was randomly generated and the fitter designs (as evaluated by objective function) were selected to breed a new generation of designs. In each iteration, the new generation of designs was created by randomly exchanging material composition characteristics within pairs of selected designs from the old generation. At this point the deformation of the designed beam under the prescribed load was converged to the defined deformation profile with the value of objective function converging to 4x10-3mm.

References and Notes

[1] Hook, A. L., Chang, C.-Y., Yang, J., Atkinson, S., Langer, R., Anderson, D. G., Davies, M. C., Williams, P. & Alexander, M. R. Discovery of Novel Materials with Broad Resistance to Bacterial Attachment Using Combinatorial Polymer Microarrays. Adv. Mater. 25, 2542-2547, **2013**

[2] Hook, A. L., Chang, C.-Y., Yang, J., Luckett, J., Cockayne, A., Atkinson, S., Mei, Y., Bayston, R., Irvine, D. J., Langer, R., Anderson, D. G., Williams, P., Davies, M. C. & Alexander, M.R. Combinatorial discovery of polymers resistant to bacterial attachment Nat. Biotechnol. 30(9), 868-875, **2012**

[3] Mei Y, Saha K, Bogatyrev S R, Yang J., Hook A.L., Kalcioglu I., Cho S., Mitalipova M., Pyzocha N., Rojas F., Van Vliet K.J., Davies M.C., Alexander M.R., Langer R., Jaenisch R., Anderson D.G.,

Combinatorial development of biomaterials for clonal growth of human pluripotent stem cells. Nat Mater, 9(9): 768-778, **2010**.

[4] Vallieres C, Hook A L, He Y, Cuzzucoli Crucitti V., Figueredo G., Davies C.R., Burroughs L., Winkler D.A., Wildman R.D., Irvine D.J., Alexander M.R., Avery S.V. Discovery of (meth) acrylate polymers that resist colonization by fungi associated with pathogenesis and biodeterioration. Sci Adv, 6(23): eaba6574, **2020**

[5] Derby, B. Inkjet printing of functional and structural materials: fluid property requirements, feature stability, and resolution. Annu. Rev. Mater. Res. 40, 395-414, **2010**

[6] de Gans, B.-J., Duineveld, P. C. & Schubert, U. S. Inkjet printing of polymers: state of the art and future developments. Adv. Mater. 16, 203-213, **2004**

[7] Skylar-Scott M A, Mueller J, Visser C W, Lewis J.A., Voxelated soft matter via multimaterial multinozzle 3D printing. Nature, 575(7782): 330-335, **2019**

[8] Han D, Yang C, Fang N X, Lee H., Rapid multi-material 3D printing with projection micro-stereolithography using dynamic fluidic control. Addi Manuf, 27: 606-615, **2019**

[9] Raviv D, Zhao W, McKnelly C, Papadopoulou A., Kadambi A., Shi B., Hirsch S., Dikovsky D., Zyracki M., Olguin C., Raskar R., Tibbits S., Active printed materials for complex self-evolving deformations. Sci Rep, 4: 7422, **2014**

[10] Ge, Q., Qi, H. J., Dunn, M. L. Active materials by four-dimension printing. Appl. Phys. Lett. 103, 131901, **2013**

[11] He Y, Foralosso R, Trindade G F, Ilchev A., Ruiz-Cantu L., Clark E.A., Khaled S., Hague R.J.M., Tuck C.J., Rose F.R.A.J., Mantovani G., Irvine D., Robert C.J., Wildman R.D., A Reactive Prodrug Ink Formulation Strategy for Inkjet 3D Printing of Controlled Release Dosage Forms and Implants. Adv Thera, 1900187, **2020**

[12] Zhang F, Saleh E, Vaithilingam J, Li Y., Tuck C.J., Hague R.J.M., Wildman R.D., He Y., Reactive material jetting of polyimide insulators for complex circuit board design. Addi Manuf, 25: 477-484, **2019**

[13] Hosny A, Keating S J, Dilley J D, Ripley B., Kelil T., Pieper S., Kolb D., Bader C., Pobloth A., Griffin M., Nezafat R., Duda G., Chiocca E.A., Stone J.R., Michaelson J.S., Dean M.N., Oxman N., Weaver J.C., From improved diagnostics to presurgical planning: high-resolution functionally graded multimaterial 3D printing of biomedical tomographic data sets. 3DP & Addi Manuf, 5(2): 103-113, **2018**

[14] Bader C, Kolb D, Weaver J C, Sharma S., Hosny A., Costa J., Oxman N., Making data matter: Voxel printing for the digital fabrication of data across scales and domains. Sci adv, 4(5): eaas8652, **2018**

[15] He Y., Begines B., Luckett J., Dubern J.F., Hook A.L., Prina E., Rose F.R.A.J., Tuck C.J., Hague R.J.M., Irvine D.J., Williams P., Alexander M.R., Wildman R.D., Manufacturing suing Cell-instructive Materials: 3D Inkjet Printing of Bespoke Medical Devices, (preprint available in Biorxiv)

[16] Costerton J W, Stewart P S, Greenberg E P. Bacterial biofilms: a common cause of persistent infections. Science, 284(5418): 1318-1322, **1999**

[17] Magill S S, Edwards J R, Bamberg W, Beldavs Z.G., Dumyati G., Kainer M.A., Lynfield R., Moloney M., MacAllister-Hollod L., Nadle J., Ray S.M., Thompson D.L., Wilson L.E., Fridkin S.K., Multistate point-prevalence survey of health care–associated infections. N Engl J Med, 370(13): 1198-1208, **2014**

[18] Lee D K. Drug-eluting stent in malignant biliary obstruction. J Hepatobiliary Pancreat Sci, 16(5): 628-632, **2009**

[19] Zhou Z, Yao Q, Li L, Zhang X., Wei B., Yuan L, Wang L., Antimicrobial activity of 3D-printed poly (ε-caprolactone)(PCL) composite scaffolds presenting vancomycin-loaded polylactic acid-glycolic acid (PLGA) microspheres. Med Sci Mon Int Med J Exp Clin Res, 24: 6934, **2018**

[20] Inzana J A, Trombetta R P, Schwarz E M, Kate S.L., Award H.A., 3D printed bioceramics for dual antibiotic delivery to treat implant-associated bone infection. Eur Cells Mater, 30: 232, **2015**

[21] Shankar P R. Book review: tackling drug-resistant infections globally. Archives of Pharmacy Practice, 7(3): 110-111, **2016**

[22] Adlington K, Nguyen N T, Eaves E, YangJ., Chang C., Li J., Gower A.L., Stimpson A., Anderson D.G., Langer R., Davies M.C., Hook A.L., Williams P., Alexander M.R., Irvine D.J., Application of targeted molecular and material property optimization to bacterial attachment-resistant (Meth) acrylate polymers. Biomacromolecules, 17(9): 2830-2838, **2016**

[23] Trindade G F, Abel M L, Lowe C, Tshulu R., Watts J.F., A time-of-flight secondary ion mass spectrometry/multivariate analysis (ToF-SIMS/MVA) approach to identify phase segregation in blends of incompatible but extremely similar resins. Anal. Chem, 90(6): 3936-3941, **2018**

[24] Passarelli M K, Wang J, Mohammadi A S, Trouillon R., Gilmore I., EwingA.G., Development of an organic lateral resolution test device for imaging mass spectrometry. Anal. Chem, 86(19): 9473-9480, **2014**

[25] Seah M P. Resolution parameters for model functions used in surface analysis. Surf Interface Anal, 33(12): 950-953, **2002**

[26] Brouqui P, Rousseau M C, Stein A, Drancourt M., Raoult D., Treatment of Pseudomonas aeruginosa-infected orthopedic prostheses with ceftazidime-ciprofloxacin antibiotic combination. Antimicrob. Agents Chemother., , 39(11): 2423-2425, **1995**

[27] Salvati E A, Robinson R P, Zeno S M, Koslin B.L., Brause B.D., Wilson P.D.Infection rates after 3175 total hip and total knee replacements performed with and without a horizontal unidirectional filtered air-flow system. J Bone Joint Surg. American volume, 64(4): 525-535, **1982**

[28] ISO 10993-5:2009. Biological evaluation of medical devices -- Part 5: Tests for in vitro cytotoxicity, **2009**

[29] Wagner M A, Huang J L, Okle P, Paik J., Spolenak R., Hinges for origami-inspired structures by multimaterial additive manufacturing. Mat & Des, 108643, **2020**

[30] Mao Y, Yu K, Isakov M S, Wu J., Dunn M., Qi H.J., Sequential self-folding structures by 3D printed digital shape memory polymers. Sci rep, 5: 13616, **2015**

[31] Ge Q, Dunn C K, Qi H J, Dunn M.L., Active origami by 4D printing. Smart Mater Struct, 23(9): 094007, **2014**

[32] Gabriel Y.H. Choong, Alessia Canciani, Davide S.A. De Focatiis, An adaptable flexural test fixture for miniaturised polymer specimens, Polym Test, 85, 106430, **2020**

[33] Passarelli M K, Pirkl A, Moellers R, Grinfeld D., Kollmer F., Havelund R., Newman C.F., Marshall P.S., Arlinghaus H., Alexander M.R., West A., Horning S., Niehuis E., Makarov A., Dollery C.T., Gilmore I.S., The 3D OrbiSIMS—label-free metabolic imaging with subcellular lateral resolution and high mass-resolving power[J]. Nat methods, 14(12): 1175, **2017**

[34] Trindade G F, Abel M L, Watts J F. simsMVA: A tool for multivariate analysis of ToF-SIMS datasets. Chemometr Intell Lab, 182: 180-187, **2018**

[35] Keenan M R, Smentkowski V S. The statistics of ToF-SIMS data revisited and introduction of the empirical Poisson correction. Surf Interface Anal, 48(4): 218-225, **2016**

[36] Heydorn A, Nielsen A T, Hentzer M, Sternberg C., Givskov M., Ersboll B.K., Molin S., Quantification of biofilm structures by the novel computer program COMSTAT. Microbiology, 146(10): 2395-2407, **2000**

[37] Pusnik M, Imeri M, Deppierraz G, Bruinink A., Zinn M., The agar diffusion scratch assay-A novel method to assess the bioactive and cytotoxic potential of new materials and compounds. Sci rep, 6: 20854, **2016**

Acknowledgments

YH, MA, RW, CT, RH, CFT, CR and BB were funded by Engineering and Physical Sciences Research Council grants EP/I033335/2, EP/N024818/1 and EP/P031684/1, EP and FR by EP/L015072/1 and MRA, PW, J-FD by the Wellcome Trust Senior Investigator Joint Awards to 103882/Z/14/Z and 103884/Z/14/Z. Funding for open access charge was provided by UK Research and Innovation.

The manuscript was written with contributions of all authors. The majority of the experimental work was carried out by YH and BB. Support for 3D printing was provided by RW, CT and JL. J-FD and AH conducted the bacterial biofilm assays overseen by PW and MRA. Cytotoxicity experiments were conducted by EP under the supervision of FR. Chemical characterisation and materials understanding was performed by GFT and supported by CR, RH, DI and MRA. Custom flexural fixture was developed by GC and DDF, and data analysis was supported by GC and DDF. Modelling and optimisation were performed by MA and overseen by IA. The work was conceived and organized by RW.

Figures and Tables

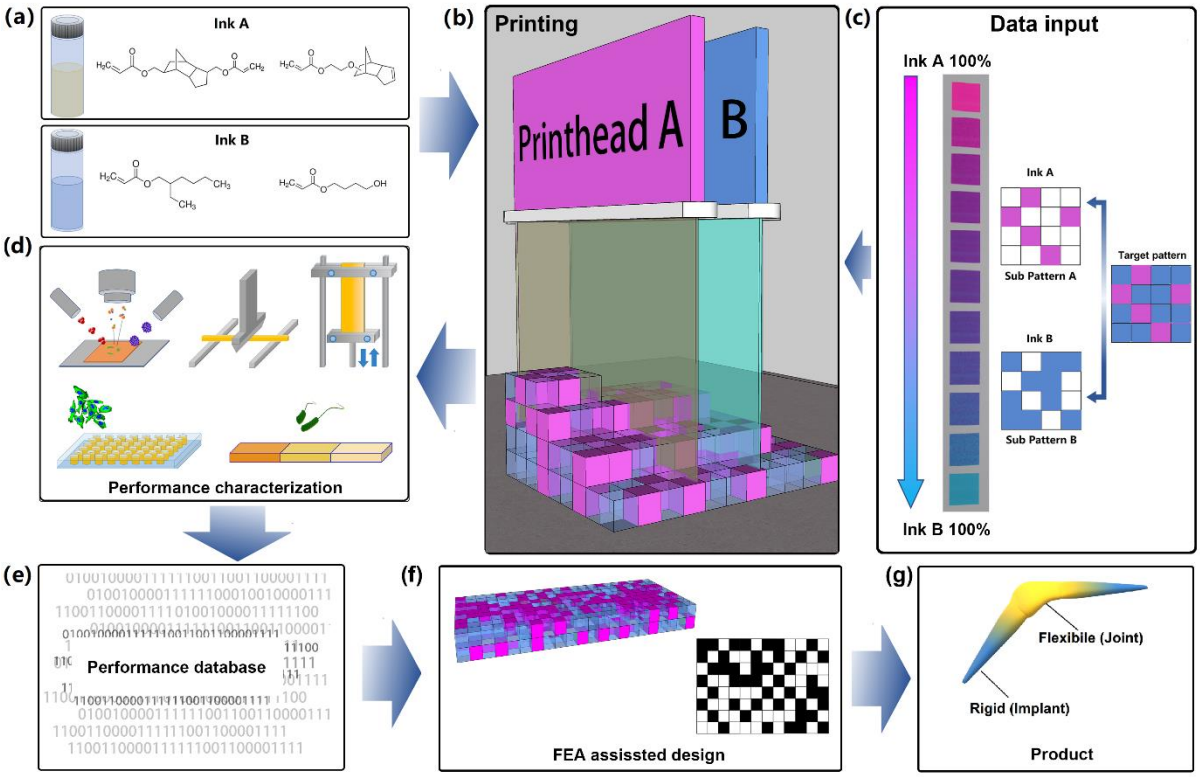

***Fig. 1**: **Schematic approach of the methodology followed to develop, 3D print and characterise bespoke biofilm inhibiting materials**. **(a)** Four monomers were chosen from an existing database to obtain two biofilm resistant materials with highly differentiated moduli. **(b)** MM-IJ3DP was achieved with a dual inkjet printing unit and a UV lamp to trigger the polymerisation after ink deposition. **(c)** A pseudorandomized printing strategy used to produce composites with choice of modulus, where complementary sub patterns were generated for ink A and ink B components, where each was the inverse of the other. **d)** Tensile and three point bend testing to determine mechanical properties, Time-of-flight secondary ion mass spectrometry (ToF-SIMS) to determine chemical composition, and bacterial biofilm inhibition and cell viability assays to assess the physical and biological performance of the MM-IJ3DP printed devices with proposed bio-instructive formulations. **e)** The performance of specimens with different compositions were collected together to form a database. **f)** A finite element analysis coupled with a genetic algorithm was performed to design specimens with required the performance on the basis of the composite properties from the database; **g)** A device exemplar was manufactured.*

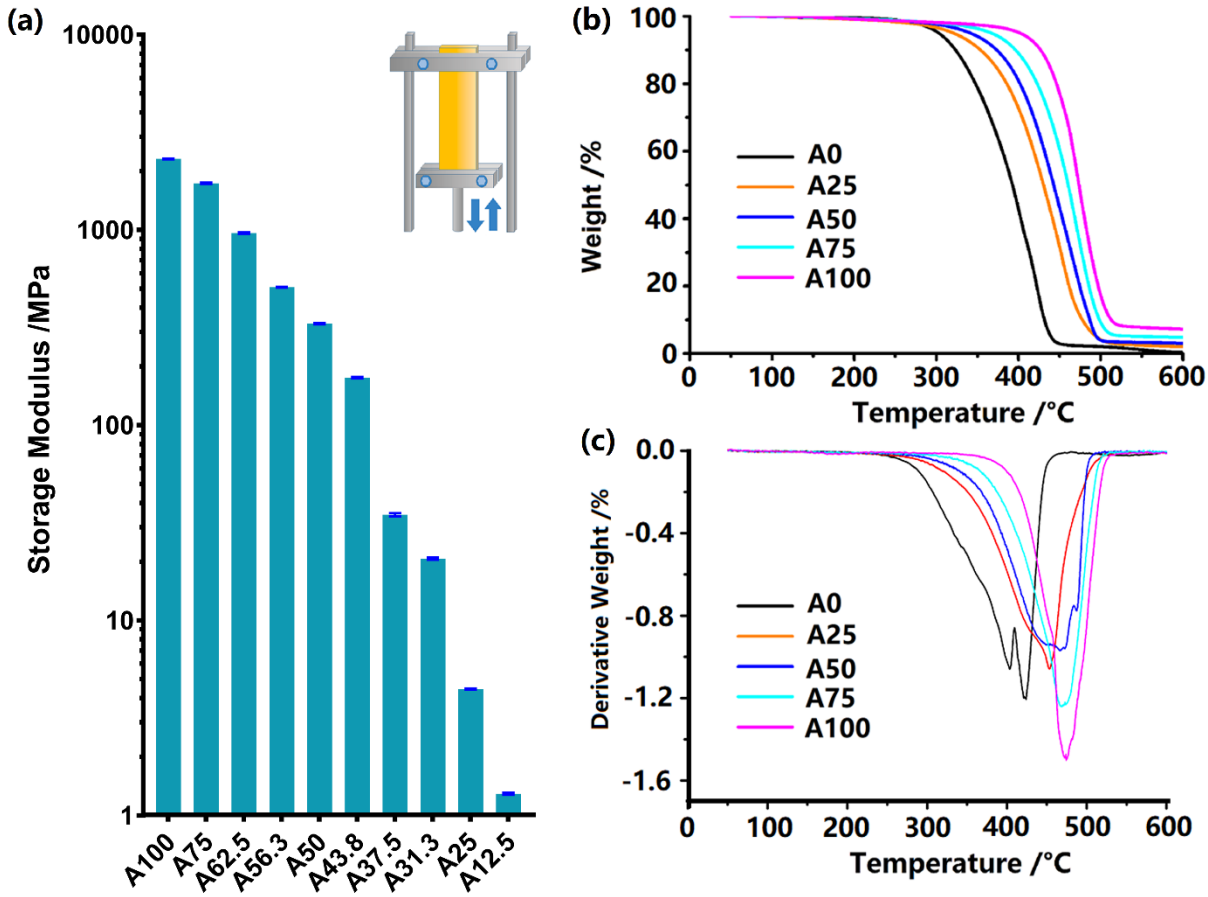

***Fig. 2**: **Preliminary assessment of polymer composite specimens with different ratios of ink A and B**: **a)** dynamic mechanical analysis (DMA) was performed and storage modulus with 10 different compositions were measured (Mean ± Standard Deviation, n=3); **b)** thermal gravity analysis (TGA) was carried out for 5 different compositions within a temperature range of 35°C to 600°C; **c)** derivative curve of the TGA to show the decomposition temperature shifting for the MM-IJ3DP printed structure.*

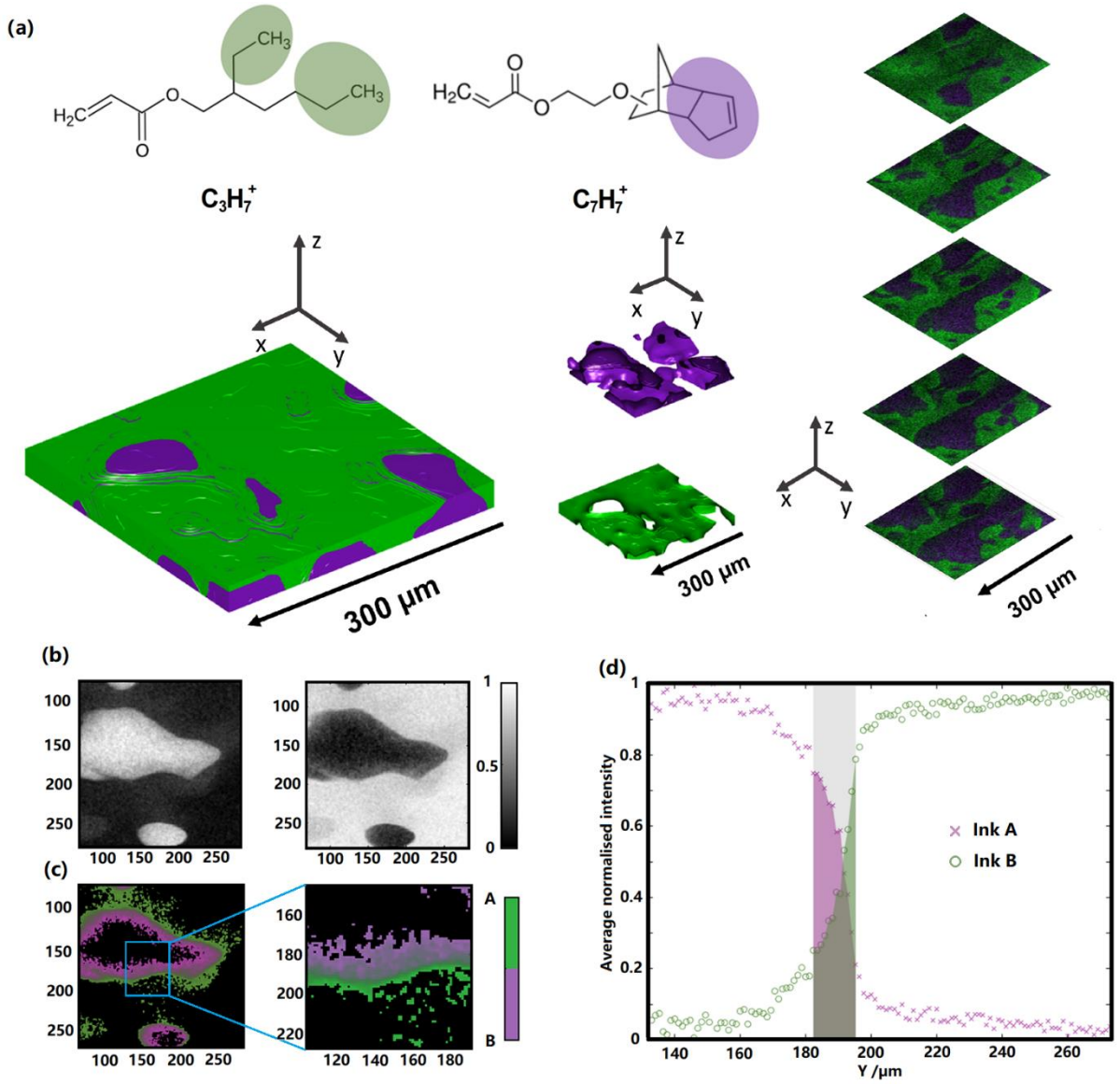

***Fig. 3: ToF-SIMS analysis of potential phase separation and interaction between the two printed ink A and B**: **a)** results showing exclusive characteristic peaks for each formulation and their 3D distribution within an approximate 300 µm x 300 µm x 10 µm volume (ink A in purple and ink B in green, droplet size ~90 µm); **b)** Intensity distribution of NMF endmembers representing ink A (left) and ink B (right); **c)** Interface region with intensity between 20 % and 80 % of the maximum for each ink. Blue rectangle represents area for the Y axis linescan in d); **d)** Average intensity distribution inks within the blue rectangle in c). Hashed area represents the interface region.*

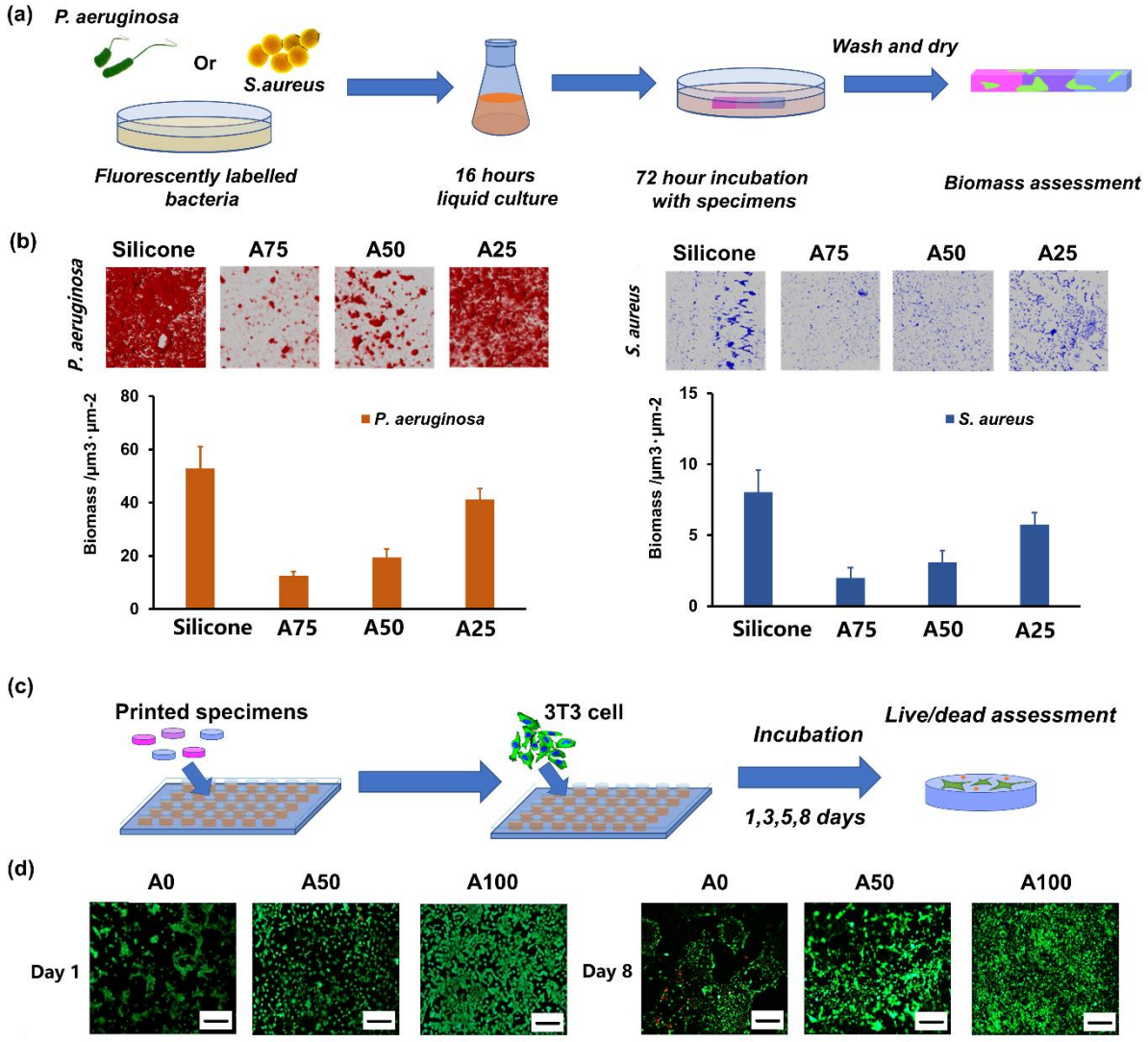

***Fig. 4:Assessment of bacterial biofilm resistance and mammalian cell biocompatibility of the printed structures**: **a)** Bacterial biofilm formation on printed sectioned samples containing composition of A25, A50, A75 were tested with silicone rubber as a reference; **b)** The biofilm biomass of* P. aeruginosa *and* S. aureus *was determined after 72h §incubation. Mean ± Standard Deviation, n = 3; Each image is 512 x 512 µm^2. Fluorescent micrographs of mCherry-labelled P. aeruginosa (red) and GFP-labelled S. aureus (blue) growing on each surface are shown (bottom). **c)** Live/Dead® cell viability assay where live cells were stained with Calcein-AM (green) and dead cells with EthD-1 (red), **d)** cell performance on the top surface of the sample were emanated fluorescent microscope, the data at Day 1 and Day 8 on A0, A50 and A100 are shown here and scale bar is 200 µm.*

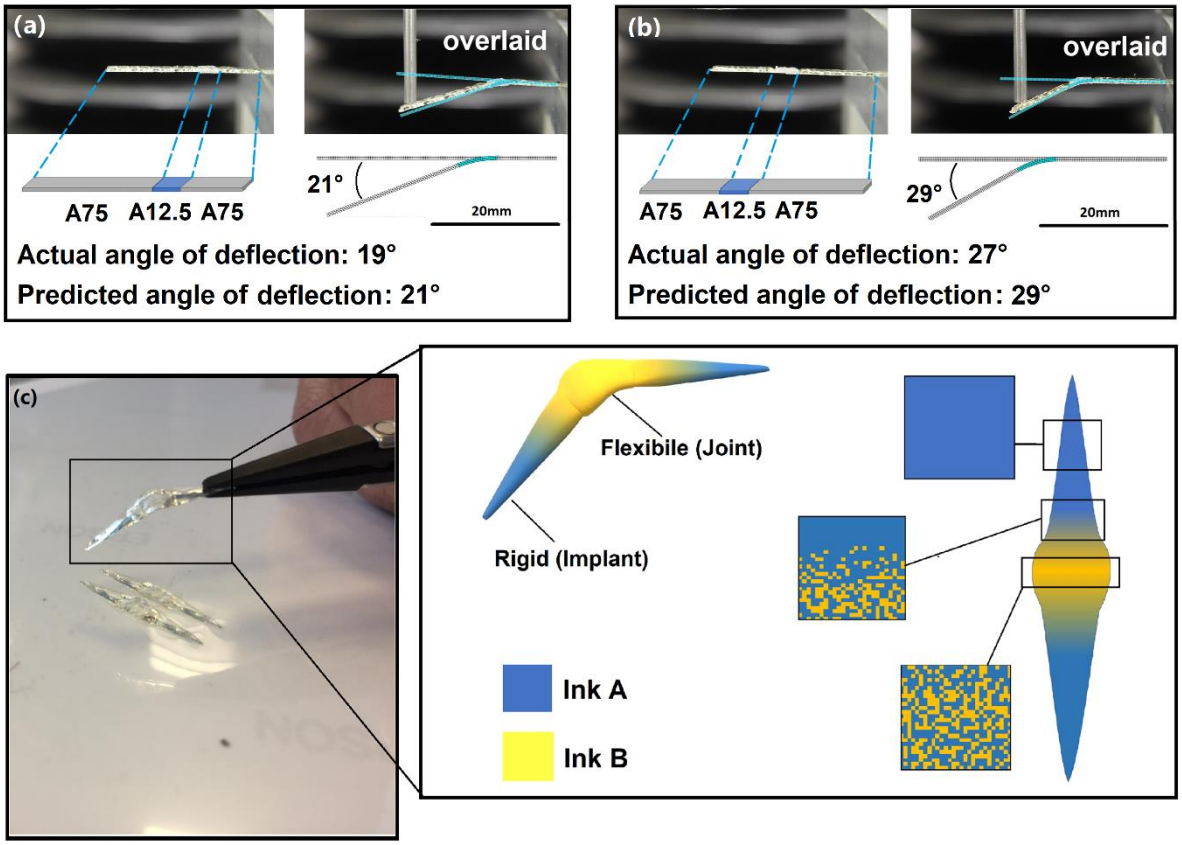

Fig. 5: Exemplar of designing the cantilever bending profile by two regions of polymer composites*: A75 (grey) and A12.5 (blue) with customized A12.5 (blue) locations, the left edge of the A12.5 region was 15mm* ***(a)*** *and 10mm* ***(b)*** *away from the free end; tests were carried out by applying 5 mm deflection on its free-end and the predicted deformation is overlaid with experiment data;* ***c)*** *A printed example for a potential application of multi-material inkjet printed biofilm resistant medical device: finger implant.*

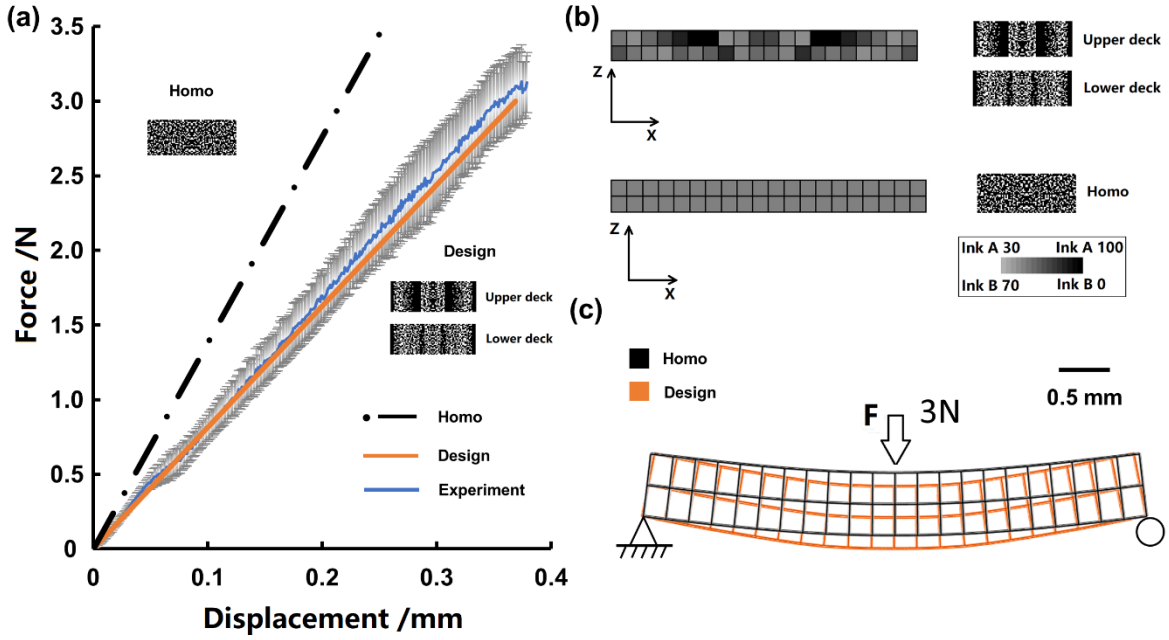

Fig. 6: Multi-material cantilever structure printed with MM-IJ3DP process: *beam specimen printed following the digital design generated from a computational model established in this study:* ***a)*** *comparison of the mechanical performance between the standard homogeneous cantilever, simulation and experimental (Mean ± Standard Deviation, n = 8)****; b)*** *FEA assisted design of cantilever structure versus homogeneous one;* ***c)*** *comparison of deflection between the two cantilevers under 3N loading*

Supplementary Materials for

Exploiting generative design for multi-material inkjet 3D printed cell instructive, bacterial biofilm resistant composites

Yinfeng He[1]▪, Belen Begines[2]▪, Gustavo F. Trindade[1,3], Meisam Abdi[4], Jean-Frédéric Dubern[5], Elisabetta Prina[3], Andrew L. Hook[3], Gabriel Choong[1], Javier Ledesma[1], Christopher J. Tuck[1], Felicity Rose[6], Richard Hague[1], Clive J. Roberts[3], Davide De Focatiis[1], Ian A. Ashcroft[1], Paul Williams[5], Derek J. Irvine[1], Morgan R. Alexander[3], Ricky D. Wildman[1]

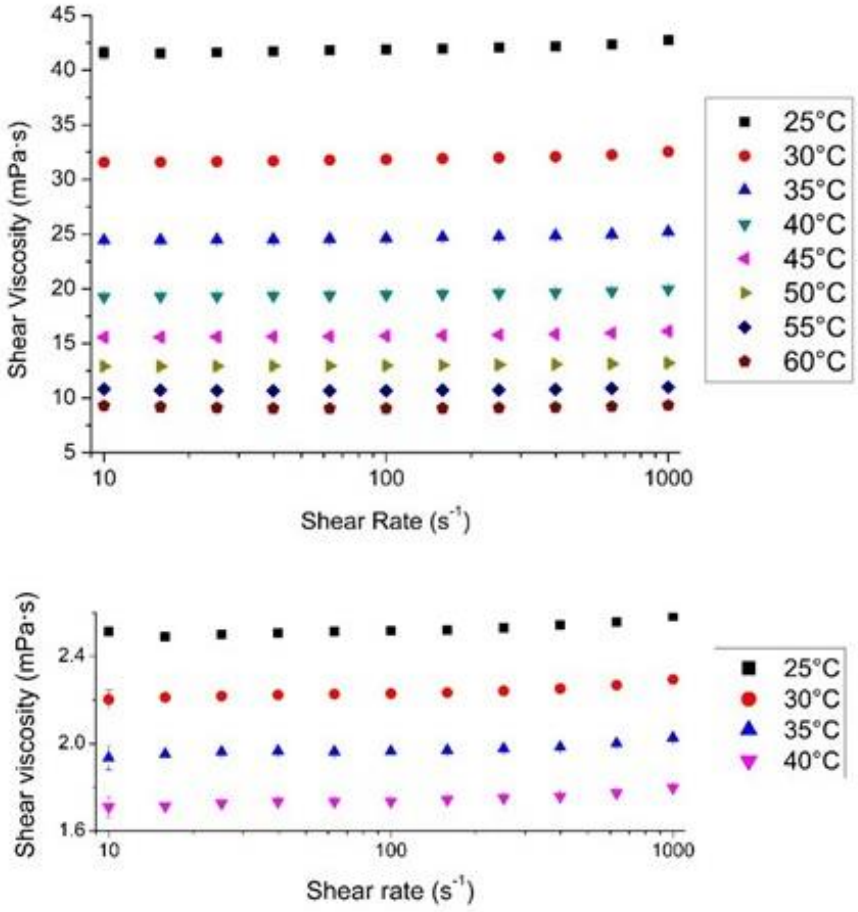

Fig. S1: Viscosity of ink A (top) and ink B (bottom) are measured using a cone plate system, in a shear rate range from 10 s^{-1} to 1000 s^{-1}, the temperatures were chosen from room temperature up to the printing temperature with an interval of 5°C , the data are shown as mean±standard deviation, n = 3.

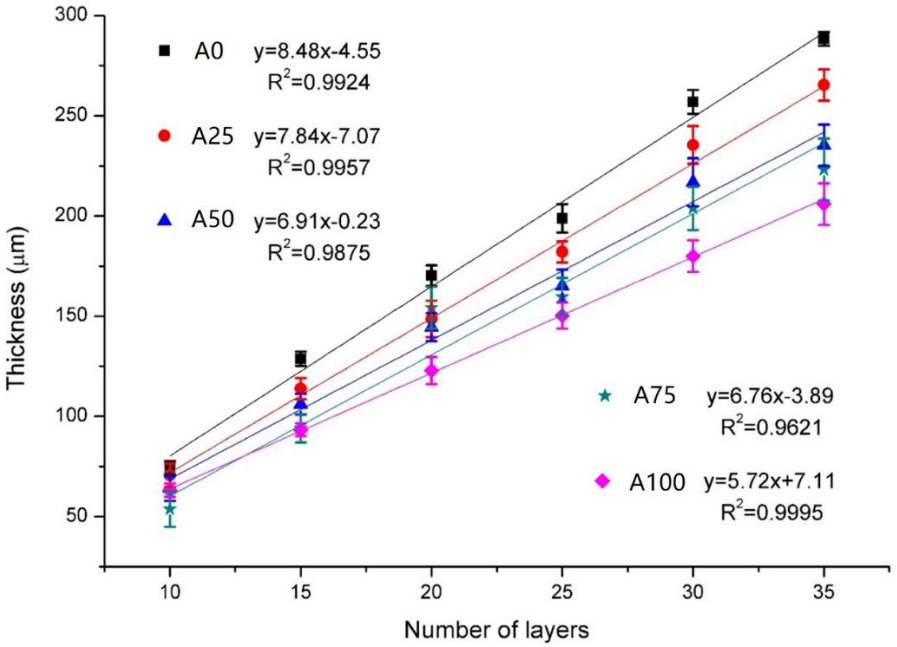

Fig. S2: The average layer thickness of the printed composites were estimated by applying simple linear regression to measured specimens height consisted of 10 to 35 layers. The data is presented as mean ± standard deviation, n = 3

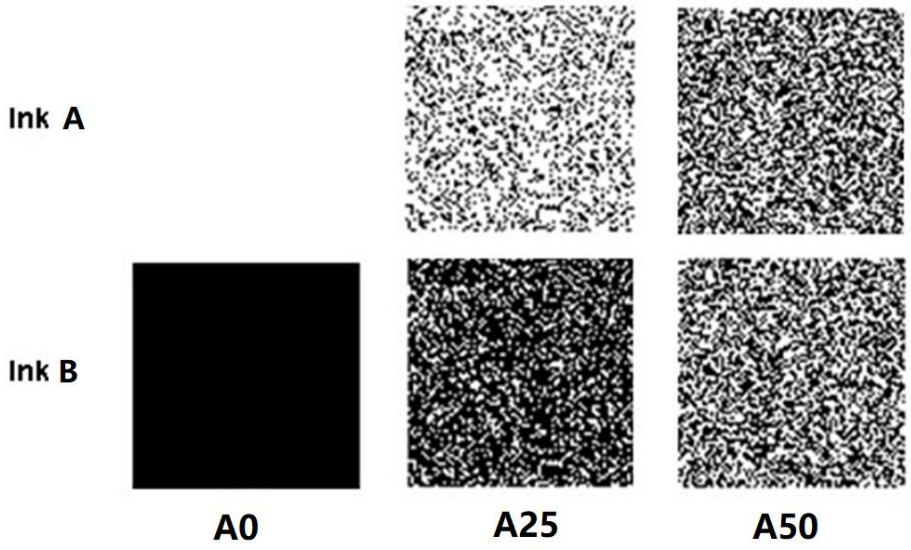

Fig. S3: Examples of Sub-pattern bitmaps for ink A and B are shown above, compositions of A0, A25 and A50 were chosen as exemplar and a simple square patten was used, where every black pixel represent the correlated ink droplet printed.

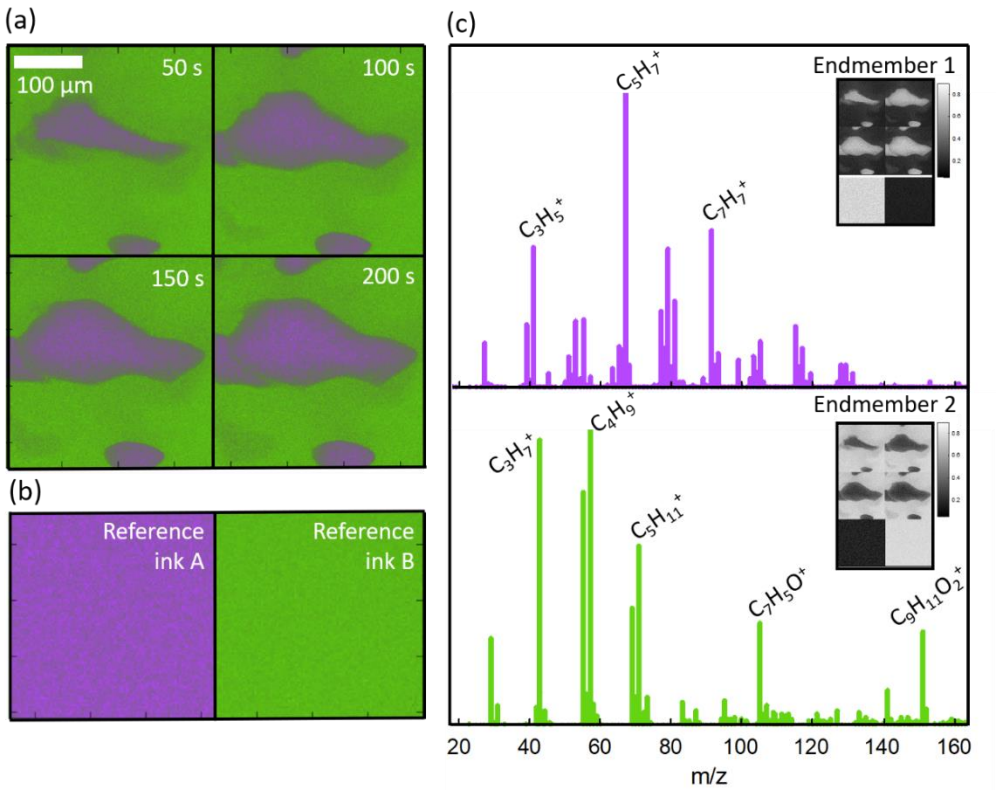

Fig. S4: Output of non-negative matrix factorisation analysis. (a) Overlay of endmembers intensity distribution of ToF-SIMS mapping data at different sputter times. (b) Endmember intensities for reference samples printed by pure inks A and B. (c) Peaks comprising endmembers 1 (ink A, purple) and 2 (Ink B, green).

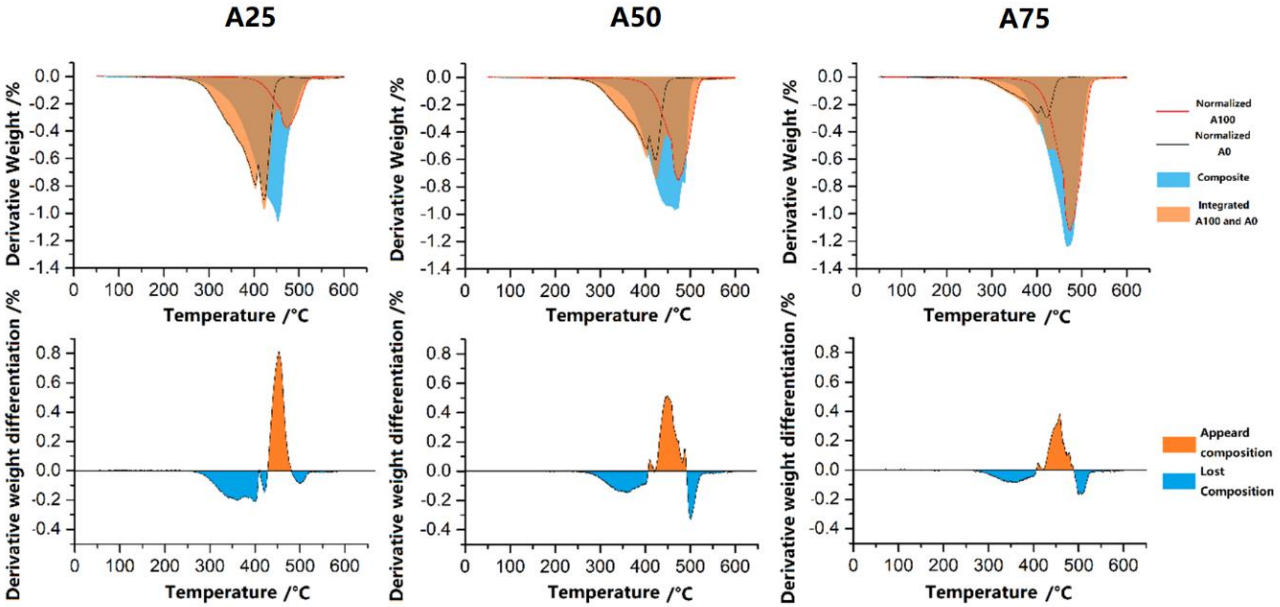

Fig. S5: The comparison of derivative TGA curves for samples A25, A50 and A75. The upper row compares the addition of curves for A0 and A100 at proportions equivalent to A25, A50 and A75, with the curves obtained for A25, A50 and A75. The bottom row shows the differences where blue represents signals that are not present in the A25, A50 and A75 composites curves and orange represents signals that appear only in the composites samples.

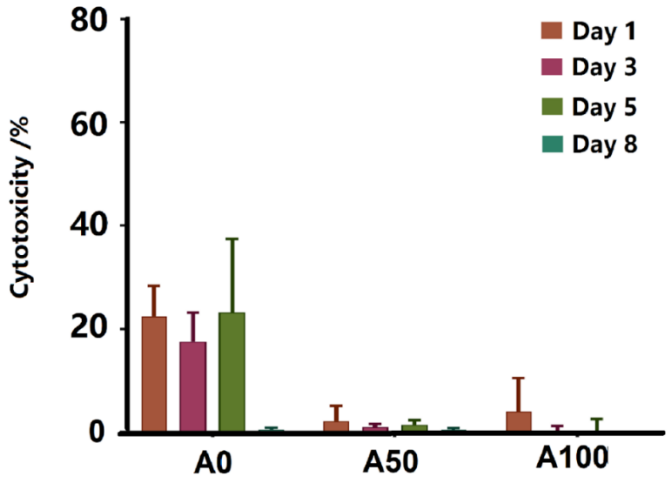

Fig. S6: Comparison of cytotoxicity (%) for a selection of printed composites (A0, A50 and A100) on different days, the tests were performed using LDH assay and immortalized NIH 3T3 mouse embryonic fibroblast cells, the data are presented as mean ± standard deviation, n = 3

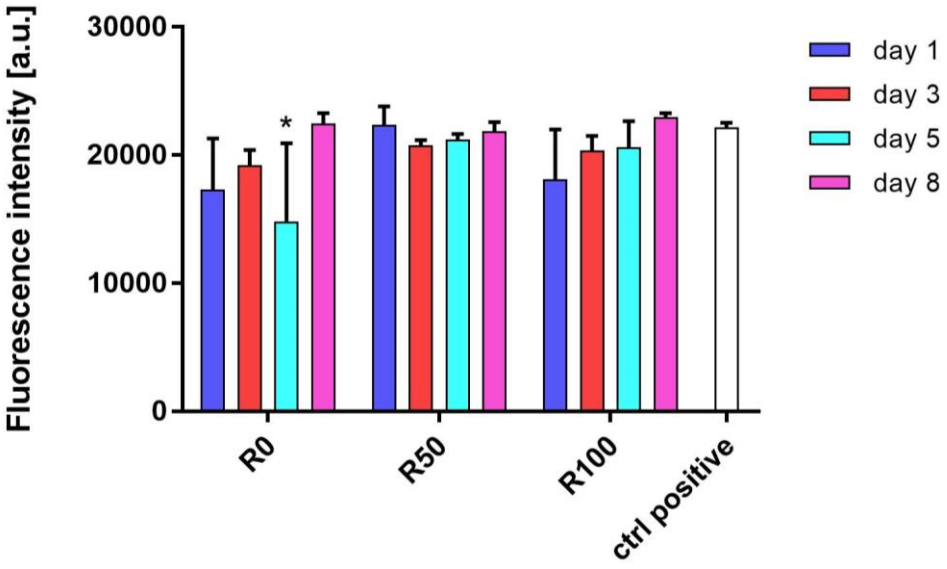

Fig. S7: Cumulative cell cytotoxicity measured by PrestoBlue. At each time point, conditioned medium extracts were collected and to culture 3T3 cells for 24 h. The error bars equal ± one standard deviation unit, n = 5. Statistically significant difference from the control (*p ≤0.05), two-way ANOVA with post-hoc Tukey's test.

Table S1: Glass transition point of the homopolymer prepared from each chosen monomer. The sample were prepared by UV polymerization in a vial and tested by DSC at a heating rate of 5°C/minutes and temperature range of -85°C to 200°C

Formulation	**Glass transition point (°C)**
Poly-TCDMDA	160°C
Poly-EGDPEA	19°C
Poly-EHA	-70°C
Poly-HBA	-65°C

Table S2: Printing parameters and jetting waveform of the two ink formulations (A and B) for printing on the Pixdro LP50 platform.

Inks	**Pulseshape**			**Voltage (v)**	**Ink Pressure (mbar)**	**Drop Spacing (μm)**
	Rising Edge (μs)	Peak (μs)	Falling Edge (μs)			
A	2	4	2	90	-20	70
B	1	4	10	83	-18	70

Table S3: Thermal properties of representative formulations measured by TGA, ^{0}Td is the temperature where the onset of decomposition was observed, $^{max}T_d$ is the point where a peak is observed in the derivative curve of the TGA test, and each temperature represents one observed peak on the curve.

Formulation	**Temperature**	
	^{o}Td (ºC)	^{max}Td (ºC)
A0	317	397/414
A25	348	436/453
A50	368	449/462/480
A75	391	466
A100	422	468